Improving the quantification of deuterium in zirconium alloy atom probe tomography data using existing analysis methods

Brief Title: Improving deuterium quantification in APT data

Authors and Institutions:

Megan E. Jones [a], Andrew J. London [b], Andrew J. Breen [c, d], Paul D. Styman [e],

Shyam Sikotra [f], Michael P. Moody [a] and Daniel Haley [a]

[a] Department of Materials, University of Oxford, Parks Road, Oxford OX1 3PH, UK

[b] UK Atomic Energy Authority, Culham Science Centre, Oxfordshire OX14 3DB, UK

[c] Australian Centre for Microscopy & Microanalysis and School of Aerospace, Mechanical and Mechatronic Engineering, The University of Sydney, NSW 2006, Australia

[d] Max-Planck-Institut für Eisenforschung, Max-Planck-Straße 1, Düsseldorf, Germany

[e] National Nuclear Laboratory, Culham Science Centre, Abingdon, OX14 3DB, UK

[f] Rolls-Royce Plc, PO Box 2000, Raynesway, Derby, DE21 7XX, UK

Corresponding Author:

Megan E. Jones

Materials Department, University of Oxford, Parks Road, Oxford, OX1 3PH

Telephone: +44(0)1865 273 634

Fax: +44 (0)1865 273789

Email: megan.jones2@materials.ox.ac.uk

Abstract

Zirconium alloys are common fuel claddings in nuclear fission reactors and are susceptible to the effects of hydrogen embrittlement. There is a need to be able to detect and image hydrogen at the atomic scale to gain the experimental evidence necessary to fully understand hydrogen embrittlement. Through the use of deuterium tracers, Atom Probe Tomography (APT) is able to detect and spatially locate hydrogen at the atomic scale. Previous works have highlighted issues with quantifying deuterium concentrations using APT due to complex peak overlaps in the mass-to-charge-state ratio spectrum between molecular hydrogen and deuterium (H_2 and D). In this work, we use new methods to analyse historic and simulated atom probe data, by applying currently available data analysis tools, to optimise solving peak overlaps to improve the quantification of deuterium. This method has been applied to literature data to quantify the deuterium concentrations in a concentration line profile across an α-Zr/ deuteride interface.

Key Words

Nuclear materials, zirconium alloys, atom probe tomography, quantification, peak overlaps, deuterium, hydrogen embrittlement

1 Introduction

Zirconium alloys are used as the fuel cladding in water-cooled nuclear fission reactors due to their corrosion resistance, adequate mechanical properties at operating conditions and a low thermal neutron cross section (Banerjee, 2001). The

interaction of the coolant water with the alloy leads to the formation of an oxide layer and the production of hydrogen, some of which is absorbed by the cladding (Motta et al., 2015). Hydrogen absorption by these alloys is an issue due to the alloys' susceptibility to hydrogen embrittlement by the formation of hydrides and crack propagation via delayed hydride cracking, creating potential issues during the long-term storage of spent fuel.

Two common sets of zirconium alloys are used: Zircaloy series, Zr-Sn alloys and Zr-Nb alloys such as ZIRLO. Zircaloy-4 is used in structural components in light water reactors. Zr-Nb alloys have been developed to have improved properties such as corrosion resistance and hydrogen pick up (Motta et al., 2015). The improved performance of Zr-Nb alloys has led to increased characterisation in these alloys. However, in both sets of alloys, hydrogen embrittlement is a life-limiting factor for fuel rods and understanding hydrogen pick up and trapping at the nanoscale has been identified as a key route to enhancing fuel life (Couet et al., 2014; Motta et al., 2019; Ensor et al., 2017)

Our understanding of hydrogen-related phenomena is limited due to the difficulties of detecting and imaging hydrogen with conventional electron and X-ray based techniques (Meyer et al., 2008). Methods used to detect and quantify hydrogen include nanoscale secondary ion mass spectrometry (Jones et al., 2021; Li et al., 2020), time-of-flight secondary ion mass spectrometry (Jiang et al., 2020) optical emission spectroscopy techniques such as laser induced breakdown spectroscopy (Kautz et al., 2021; Pardede et al., 2019) and LECO hydrogen hot vacuum extraction (Ensor et al., 2017) but have not yielded all of the necessary experimental data. Atom Probe Tomography (APT) has nanometre level spatial resolution and high chemical sensitivity making it a viable tool for hydrogen analysis.

Environmental hydrogen, not originating from the material's microstructure, is routinely observed in APT datasets and arises from hydrogen either adsorbed onto the sample, or located within the analysis chamber and ionised during the experiment (Sundell et al., 2013). During data analysis, it is normally not possible to identify the origin of the hydrogen, constituent or environmental, thus ultimately obscuring the positive detection of hydrogen originating from within the sample (Kunimune et al., 2016; Sepehri-Amin et al., 2011; Breen et al., 2018).

To circumvent this issue, deuterium (^{2}H, for which we will be using the symbol 'D' in this text) has been used as a tracer; the natural isotopic abundance is low (0.015%), therefore any detected deuterium can be assumed to have originated from the sample (Takahashi et al., 2010; Gemma et al., 2009; Chen et al., 2017). The addition of deuterium can however lead to peak overlaps (peaks from differing species overlap in mass-to-charge-state ratio) between deuterium (D^{+}) molecular protium ($^{1}H_{2}^{+}$) in the APT mass spectrum. In some cases, the APT analysis of deuterated materials have been conducted using voltage pulsing to prevent these unwanted mass-peak overlaps (D-H_2 overlap); however, this limits the range of samples that can be readily analysed. Importantly, zirconium alloy specimens are less viable for successful APT analysis when subjected to the stresses induced by voltage pulsing and thus this material is typically analysed in laser pulsing mode (Wadman et al., 1988). Due to the lower electrostatic fields in laser-pulsing mode, the evaporation of molecular ions is common, including H_2, ZrH and ZrH_2 ions (Tsong et al., 1983). These molecular ions are present in peak overlaps in the mass spectrum, therefore to calculate accurate compositions, the relative contribution of each species in each respective peak must be calculated. Thus, even with deuterium

tracing, to quantify deuterium concentrations these peak overlaps must be solved accurately.

Peak overlaps in the mass spectrum occur when ions have similar atomic masses; either when the peaks corresponding to more than one ion directly overlap in the mass spectrum (direct peak overlap) or where a smaller peak overlaps with the tail of the proceeding peak (tail overlap) (London et al., 2017). In situations where peak overlaps occur, it is necessary to estimate the number of counts each ionic species contributes to a peak, known as peak overlap solving. If there are at least as many peaks as there are ionic species in each group of overlaps then we can use the natural isotopic abundances of the ion and the other peaks in the overlap problem to estimate the number of counts each ion contributes to each peak. Peak overlaps occur in zirconium alloys occur between Zr and ZrH_x type ions and, in Nb containing alloys such as ZIRLO, Nb is also present in peak overlaps. Nb ions overlap with ZrH ions (^{93}Nb and $^{92}Zr^{1}H$), as shown in the overlap maps in the supplementary information. All peak overlaps, not only those involving deuterium containing ions, must be accurately solved to obtain robust compositional information. Previous work analysed the growth front of a grain boundary deuteride, the composition of which was found by solving overlaps using a least squares approach (Breen et al., 2018; Mouton et al., 2019). The maximum likelihood estimation (MLE) has been used to mathematically solve peak overlaps in APT data (London et al., 2017), as MLE is advantageous to use when dealing with low counts (Maus et al., 2001). In order to analyse trapped solute deuterium, we need to accurately deal with low counts of deuterium. To this end, we examine the effectiveness of different peak overlap solving tools, including the use of MLE based methods, as applied to simulated and literature data.

2. Materials and Methods

This work re-analyses historical data and uses simulated data. The experimental parameters from the earlier studies are given below for convenience. A full list of the experimental datasets used in this work can be found in the supplementary data and raw data is available on Oxford Research Archive (see Data Statement for more information). APT reconstructions from these experimental datasets were created using IVAS (Version 3.8.4, CAMECA), using the initial tip radius as obtained from the specimen bias voltage curve. Compositional analyses were performed using IVAS or AtomProbeLab (atomprobelab.sourceforge.net, version 0.2.2, Revision 43547cca1144), with AtomProbeLab using MLE. A minimum isotopic abundance of 0.02% was used to exclude naturally occurring deuterium from composition calculations.

2.1 Nb composition verification between software packages

For the Nb composition analysis, below, this uses the data of Hudson re-analysing with the MLE method (Hudson, 2011). In Hudson's work, a ZIRLO needle (nominal composition cannot be quoted for proprietary reasons) was prepared for APT analysis by electropolishing using a 25%-perchloric acid (60%) in acetic acid (100%) initially, and fine polished using 2%-perchloric acid (60%) in 98%-2-butoxyethanol, using the method described in (Hudson, 2011). The needle was further sharpened using a focused ion beam. Data was collected using a Local Electrode Atom Probe (LEAP) 3000X HR at 60 K, using a laser pulse frequency of 200 kHz. The laser energy was varied between 0.2-0.6 nJ at intervals of 0.05 nJ. 1 million ions were collected at each laser energy (Figure 1).

2.2 Peak count quantification

Figure 2 shows mass spectra produced for the entire mass spectrum of composition in Table 1, modelled on the 0.6 nJ data from Figure 1, and a second set for the Zr 2+ charge state only (Table 2). These datasets were produced containing 1 million ~~masses~~ events, but only the mass data was used in the subsequent analysis. The masses were selected to produce both ‘real’ peak shapes and Gaussian shapes in time-of-flight space. A dataset for the whole mass spectrum was produced using ‘real’ and Gaussian peak shapes with a full width half maximum of 0.06 Da. Datasets for the 2+ charge state was produced using Gaussian peak shapes only. In mass-to-charge space, the Gaussian shaped peaks have a full width half maximum of 0.06 Da and 0.28 Da. The corresponding ionic compositions for these datasets can be found in the supplementary information.

2.3 Meta-analysis of deuterated Zircaloy-4

Existing deuterated Zircaloy-4 data was used in this analysis (Breen et al., 2018), the preparation method from this work is paraphrased as follows: Zircaloy-4 (Zr-1.5Sn-0.2Fe-0.1Cr wt.%) was electrochemically charged using 1.5 wt.% D_2SO_4 in D_2O at 65°C for 24 hours. The sample was then annealed at 400°C for 5 hours to redistribute the deuterium. Samples for APT analysis were prepared using a FEI Helios dual-beam plasma focused ion beam using the lift-out procedure by Thompson et al. (Thompson et al., 2007). A LEAP 5000 XR was used to perform APT experiments with analysis conditions of 60 pJ laser energy, 250 kHz laser pulse frequency and a temperature of 60 K.

To calculate the deuterium concentrations for the deuterated Zircaloy-4 APT data, peak overlaps in the mass spectrum need to be solved. The introduction of

deuterium to the material leads to direct peak overlaps between H_2 and D including D-H_2 overlap at 2 Da, and ZrH_2-ZrD overlaps in the 2+ charge state. These overlap problems are rank deficient, i.e. there is insufficient information to constrain the problem from the mass spectrum alone, and cannot be directly solved using conventional methods. However to improve the accuracy of deuterium quantification, it is nonetheless necessary to accurately solve the respective contribution to these peak overlaps.

A key source of error is due to the unknown H_2:H ratio. Knowing this ratio would allow us to solve the overlap at 2 Da more accurately and improve the accuracy of the overall deuterium concentration, as it allows for the number of counts in the peak at 2 Da that are H_2^+ to be calculated, meaning that any counts that are unaccounted for are D^+. To obtain this ratio, and thus provide sufficient information to solve this overlap, the environmental hydrogen detected within a number of non-deuterated APT datasets was analysed, as will be discussed in Section 3.3. These datasets were a combination of Zircaloy-4, Zr-0.2Nb, Zr-0.8Nb and Zr-2.5Nb. All of these samples were prepared using the lift out method described by Thompson et al. (Thompson et al., 2007), using either a FEI Helios dual-beam plasma focused ion beam (Zircaloy-4 samples), a Zeiss NVision dual-beam Ga focused ion beam (Zircaloy-4 and Zr-Nb alloy samples) or Zeiss Crossbeam dual-beam Ga focused ion beam (Zircaloy-4 samples). The APT experimental conditions used for these samples used laser pulse energies between 40 and 100 nJ, laser pulse frequencies of either 200 or 250 kHz and temperatures between 50 and 60 K. A full list of experimental conditions can be found in the supplementary information.

2.4 The influence of electric field on molecular H formation and the H_2:H ratio

The hydrogen and deuterium charged data used in this section is from literature (Mouton et al., 2019), where Zircaloy-4 (Zr-1.5Sn-0.2Fe-0.1Cr wt.%) was electrochemically charged with hydrogen or deuterium using 1.5 wt.% H/D_2SO4 in H/D_2O at 65°C for 24 hours. The sample was annealed at 400 °C for 5 hours to redistribute the deuterium. Samples for APT analysis were prepared using a FEI Helios dual-beam plasma focused ion beam using the lift-out procedure in (Thompson et al., 2007). APT experimental conditions of 60 pJ laser energy, 250 kHz laser pulse frequency and a temperature of 60 K were used.

3 Results

~~Our results will be presented in the following section.~~ The results presented in this section will be organised in the following manner; ~~F~~first, we will ~~shall~~ report the verification of Nb composition between different software packages using historical data. The results of peak count quantification on simulated data will then be presented before our meta-analysis of deuterated Zircaloy-4 is shown. Finally, we ~~shall~~ show data on the influence of the electric field on molecular H formation and the H_2:H ratio. The data from both the meta-analysis and the influence of the electric field on hydrogen is from the literature.

3.1 Nb composition verification between software packages

Zr-Nb alloys are commonly used in structural components of nuclear fission reactors so it is imperative we can calculate the compositions of any APT data from

these alloys correctly. The re-analysis of Hudson's data, using AtomProbeLab, gave similar results to that reported by Hudson, for all of the alloying elements except Nb. Hudson states that there is 'no clear trend in the data' (Hudson, 2011). Specifically in our preliminary analysis for Nb, an apparent increasing trend with laser energy was found, as shown in Figure 1. From the examined data, Nb appears in the 1+, 2+ and 3+ charge states, however in the 1+ and 2+ charge states there are peak overlaps with ZrH ions, as shown in Figure 2. As Nb is a key element in this alloy, finding the correct solution for the overlap group is of primary interest. Furthermore, to analyse deuterated zirconium alloys will also introduce ZrD ions into the mass spectra data, which are present in this overlap group also, a graphical representation of this can be found in the supplementary information. In his analysis, Hudson used IVAS 3.4.1, so there exists a potential mismatch between the use of AtomProbeLab and IVAS to calculate compositions as AtomProbeLab uses maximum likelihood estimation. For a full discussion of the primary methods of solving these overlap problems, specifically using a least-squares (or non-negative least-squares) or maximum likelihood approach, the reader is referred to London et al, which provides in-depth comparisons of these numerical approaches (London et al., 2017). To locate the origin of the discrepancy between AtomProbeLab and the results of Hudson, the same input masses and ranges were used for both the IVAS and AtomProbeLab analyses, limiting the difference to subsequent processing within the software.

Figure 1 shows the difference in overlap analysis results due to the use of different software packages. The confidence intervals (90%) of the MLE composition calculation were estimated (London, 2019). IVAS and AtomProbeLab do not give the same Nb concentrations at all experimental laser energies and the difference in these values has led to a different trend seen in the data. The IVAS results give no

trend with laser energy whereas the AtomProbeLab ones show an increasing Nb concentration with laser energy. The default local background subtraction parameters were used in this version of AtomProbeLab, however the Nb concentration showed some sensitivity to these settings. To further probe this discrepancy IVAS-MLE data points in Figure 1 have been calculated using the peak count information from IVAS, but the peak overlaps were instead solved using the maximum likelihood estimation approach. These data points do not show a trend in Nb concentration, indicating that the difference in trend is likely as a result of the peak quantification (counts) which are inputted, not the subsequent peak overlap solving. The mass spectrum in Figure 2 contains peak-tail overlaps between adjacent peaks, which if not handled correctly can lead to incorrect count quantification and therefore compositions.

3.2 Peak count quantification

To investigate the hypothesis that the difference in the respective handling of peak-tails between the two packages are the origin of the different reported compositions, simulated data was used. Realistic peak shapes that mimicked experimentally observed peaks were generated for this data. The resulting peak-overlap analysis results were cross-compared with the input simulation composition, the Gaussian blurred composition, and the subsequent estimations from both IVAS and ~~APL~~ AtomProbeLab.

An entire ZIRLO mass spectrum was simulated with a realistic peak shape and a Gaussian peak shape, respectively, to enable contrast between situations where peak tail overlaps did and did not occur, respectively. Peak tail overlaps arise when a smaller peak overlaps with the tail of the proceeding (lower mass-to-charge-

state ratio) peak (London et al., 2017). There was some discrepancy between the compositions of the simulated data (Table 3). However, from the cross-comparison the Gaussian model maintains the expected composition, for both AtomProbeLab and IVAS, which is not the case for the realistic peak model. In the realistic peak data, neither AtomProbeLab nor IVAS effectively accounted for the peak tail overlaps, leading to a difference between the simulated and the reported values. The IVAS reported value is, however, closer to the simulated one than that of AtomProbeLab.

The majority of the Zr, Nb and ZrH ions are present in the 2+ charge state so a second set of data containing only these peaks were simulated using a Gaussian peak shape. This enables further investigation of the peak counting and the effect of peak tails on the peak quantification. The ionic composition of the peaks was modelled on the experimental data in Figure 2 (a). Two different peak widths were used, a narrow peak width with a FWHM of 0.063 Da to simulate no peak tail overlaps as seen in Figure 3 (a) and a larger peak width (FWHM of 0.28 Da) to give rise to large peak tail overlaps shown in Figure 3 (b). A Gaussian curve was fitted to the peaks in both situations; a Gaussian curve was used as the simulated data was produced with Gaussian peak shapes. Figure 3 presents the simulated mass spectra for both peak tail situations described above, the Gaussian curve fitted to the data and the bar charts show what fraction of the total quantified counts each software calculates to be in each peak.

The bar charts in Figure 3 (c), show that when peak tails do not overlap, counts for each peak can be calculated accurately, matching the simulated counts. However, when examining the case where tail overlap occurs, the estimate deviates from simulation for both the AtomProbeLab and IVAS reported values, Figure 3 (d).

In this instance, the deviation is marked, with the simulated composition of 85.51 at. % Zr, estimated to be 95.04 at. % and 91.31 at. % (after peak overlap solving) for AtomProbeLab and IVAS respectively. The quantification of the counts in the peaks by IVAS were closer to the simulated values than AtomProbeLab but the most accurate were given by the fitted spectrum.

3.3 Meta-analysis of deuterated Zircaloy-4

Using MLE based methods, we have then investigated the calculation of deuterium concentration within deuterated Zr alloy samples. As stated above, we reanalysed an existing dataset, with the aim of improving the quantification of the deuterium component of this dataset.

In deuterated samples, deuterium is present in the mass spectrum as D^+, DH^+, D_2^+ and deuteride ions (including ZrD, ZrDH and ZrD_2). The resulting peak overlaps due to these complex ions make accurate interpretation of the mass spectra challenging. Notably, there are direct peak overlaps between D^+ and H_2^+ and between ZrD and ZrH_2 (both in 2+ and 1+ charge states) that are not solvable using conventional peak overlap solving techniques, as the problems are rank deficient. To circumvent this limitation in the previous work (Breen et al., 2018), compositions were calculated by assuming that the peak at 2 Da was entirely comprised of deuterium (D^+). It was also assumed that, as there were negligible counts of ZrH_2 in the uncharged data, all of the counts of ZrH_2/ ZrD were all ZrD. By omitting the contributions from these peaks from $^1H_2$ containing ions, deuterium concentrations are over estimated, as acknowledged in their analysis (Breen et al., 2018; Mouton et al., 2019). In the uncharged Zircaloy-4 dataset, there is negligible ZrH_2 in the uncharged data, and the assumption that there are no counts of ZrH_2 in the data has

little effect on the overall composition. This implies that, unless the ratio of Zr:ZrH_2 (excluding ZrD) is changed by several orders of magnitude by the charging process, then estimation of ZrD is largely unimpeded.

However, this is not the case at 2 Da, where the H_2:H ratio is non-negligible, ranging between 0.24 and 0.69 when calculated for non-deuterated zirconium alloy samples. Whilst the initial overlap problem is rank deficient, we can use the assumption that the ratio of H_2:H does not change as a result of the charging process to constrain the final degree of freedom in this overlap problem. Thus we can estimate the amount of deuterium in the peak at 2 Da, thereby improving the accuracy of the final deuterium concentration. A final concern is that the H_2:H ratio can vary from tip to tip, and in the absence of a paired experiment in the uncharged and charged case, this must be accounted for. To quantify the variability in this ratio, we examined historical Zr alloy datasets acquired using a LEAP 5000 XR. 24 zirconium alloy datasets were analysed to find the H_2:H ratio, which had a mean ratio of 0.41 and a standard deviation of 0.15, the detailed experimental conditions for which are shown in the supplementary information.

A peak overlap solved composition line profile across the interface was produced in similar region of the dataset (Figure 4), finally generating a profile similar to the prior work (Breen et al., 2018) which is shown in Figure 5. The upper and lower bounds for the deuterium concentration were calculated using confidence limits drawn from the H_2:H ratios $\mu \pm 2\sigma$ (0.11 and 0.71), which effectively assumes that the inter-sample variability dominates the profile error, and is Gaussian distributed.

3.4 The influence of electric field on molecular H formation and the H_2:H ratio

As previously mentioned, the H_2:H ratio can vary significantly from tip-tip. It can also vary within different regions of the same dataset and this can have significant implications for deuterium quantification since D overlaps with H_2 at 2 Da. The electric field has previously been proposed as the major cause of variations in this ratio (Breen et al., 2020), which seems logical given lower electric fields tend to promote increased molecular ion formation (Müller et al., 2011) but perhaps the relationship is not so straight forward and may also change between different material systems and analysis conditions.

To investigate this hypothesis, the amount of ions evaporating from the 1 Da and 2 Da peaks and the local electric field were compared between representative hydrogen charged and deuterium charged datasets of Zircaloy-4 collected under the same experimental parameters (60 pJ laser pulse energy, 250 kHz laser pulse frequency and 60 K). The relative charge states of a single element can be used to measure electric field (Müller et al., 2011; Kingham, 1982; Shariq et al., 2009) and as electric field increases, the number of ions evaporating at a higher charge state increases. Here the $^{90}Zr^{3+}$ /$^{90}Zr^{2+}$ ratio was used to determine relative electric field since each peak was free of any overlaps and an appreciable number of ions were evaporating at each charge state (Mouton et al., 2019). Each dataset was voxelised into 3 nm cubes and the local 1 Da and 2 Da counts and Zr^{3+} /Zr^{2+} ratio in each voxel was mapped across the reconstructed volumes, as shown in Figure 6 (a) and (b).

4 Discussion

4.1 Nb composition verification between software packages

Figure 1 shows that the IVAS-MLE data points do not show a trend in Nb concentration with varying laser energy, indicating that the difference in trend between the IVAS and AtomProbeLab results is likely as a result of the peak quantification (counts) which are inputted, not the subsequent peak overlap solving. Most notably, the data analysed here contains peak-tail overlaps between adjacent peaks, as seen in Figure 1, which if not handled correctly can lead to incorrect count quantification. NbH was not looked at in this analysis as negligible amounts of NbH were calculated to be in the data and the addition of these ions had little effect on the calculated composition.

4.2 Peak count quantification

There was a discrepancy between the simulated compositions and those calculated using IVAS and AtomProbeLab. The composition IVAS calculates for the simulated data is closer to the simulated value as a result of the number of counts in the peaks being closer to the simulated value (Figure 3). In the situation where there are no peak tail overlaps, both programs are able to calculate the correct composition (Table 3), indicating that the peak overlaps are being solved accurately. Where peak tail overlaps occur, neither software is handling these effectively, giving rise to an incorrect composition. The analyses demonstrate that if it were possible to improve the way the respective software packages handle the peak tail overlaps, both should be able to provide a more accurate measurement of composition. This

however requires quantitative improvements to the modelling of underlying peak shapes, and these models are currently limited for general application.

There is good agreement between the simulated number counts and the fitted counts in Figure 3. This demonstrates that if mass spectra were to be deconvoluted and the shape of each peak known, peak fitting could be used to calculate the total counts in the peak and a more accurate composition could be obtained. To this end, methods such as the one developed by Johnson et al. or Meisenkothen et al. could be implemented (Johnson et al., 2013; Meisenkothen et al., 2020).

The results in this section demonstrate that, without further software modifications to include peak fitting, the most accurate deuterium compositions would be obtained by using IVAS to obtain the count information. As the maximum likelihood estimation is more suitable for solving peak overlaps at low counts, using the AtomProbeLab MLE algorithm to solve peak count information derived from IVAS is the most appropriate method to solve this overlap group accurately. This is the reason this approach has been used to analyse data from (Breen et al., 2018).

4.3 Meta-analysis of deuterated Zircaloy-4

Figure 5 confirms that Sn is segregating to similar levels as found in the previous work. By comparing the deuterium profile calculated using the same assumptions as previous work to the upper and lower bounds, we can see that the previous work is in good agreement with the upper bound of the deuterium concentration. This demonstrates prior values (Breen et al., 2018) were reasonable, but positively biased.

This method is able to produce upper and lower limits for the deuterium concentrations in APT data acquired in laser mode. Whilst the assumptions in

previous works mean that measurements of deuterium concentrations were qualitative, here we demonstrate a quantitatively corrected profile for the deuterium concentration for the first time. This is enabled by a customisable peak overlap solver where it is possible to use altered isotopic abundances; in this instance deuterium was added as an additional element with 100% isotopic abundance. Future deuterium analyses and other instances where the isotopic ratios of elements are altered from the natural abundance (i.e. transmutation of alloying elements in irradiated data) require this. The ability to accurately quantify deuterium concentration will allow for additional chemical information surrounding hydrides and hydrogen distributions in materials to be analysed. This in turn would enable us to further our current understanding of hydrogen embrittlement.

4.4 The influence of electric field on molecular H formation and the H_2:H ratio

Interestingly, for the H charged case (red curve in Figure 6 (c)), the average 2 Da: 1 Da ratio (which represents H_2:H in this case) stays almost constant at approximately 0.4 - 0.5 for varying electric field, suggesting changes in electric field did not strongly influence molecular H formation. For the D charged case however, different behaviour is observed. The 2 Da: 1 Da ratio (which now represents (D +H_2):H) is higher for all electric fields as would be expected since the presence of D in this case will work to increase the numerator. The ratio also increases as electric field increases since the deuteride regions, which are significantly higher in deuterium content, evaporate at higher electric fields. It follows that any additional counts in the 2 Da peak that push the 2 Da: 1 Da ratio above 0.7-0.8, correspond to deuterium and not molecular H – this observation provides a potential way for quickly screening for the presence D in APT datasets. Further information to constrain the

H_2:H ratio, would enable further tightening of the bound on the deuterium concentrations reported Figure 5, therefore improving the quantification of deuterium.

5 Summary

Data from a laser energy optimisation study were re-analysed using AtomProbeLab and IVAS in which significantly different Nb concentrations were calculated for each laser energy depending on analysis software choice. The software choice also yielded contradictory trends in the data. By examining the number of counts each software calculated, it was found that for peaks, where peak-tail overlaps occur in the mass spectrum, such as the Zr^{2+} charge state peaks, neither IVAS nor AtomProbeLab estimated the number of counts accurately. This demonstrates the importance in handling and modelling peak tail overlaps correctly; peak fitting methods could be used to do this, which would require suitable peak shape models. If analysis is limited to existing toolsets, we find that the most accurate composition with respect to simulations is obtained when using peak count estimation from within the IVAS software packages, and combining this with MLE solving (AtomProbeLab). We further re-analysed existing Zircaloy-4 deuteride profiles, as obtained from Breen et al., demonstrating that when using additional historical Zr alloy data, we can provide accurate, quantitative bounds on Zr profiles. We find that the assumptions of zero H_2^+ present in prior works causes a slight over-estimation of the D content of this profile, which our utilisation of historical data solves, assuming similar response between non-deuterated Zr alloy datasets.

Acknowledgements

The authors would like to thank Anne Callow of the University of Oxford for the use of her data. M. E. J. acknowledges support from EPSRC, Rolls Royce Plc. and National Nuclear Laboratory. AB is grateful for funding support from the Alexander von Humboldt Stiftung and the characterisation facilities at the Max-Planck-Institut für Eisenforschung GmbH. D. H. acknowledges EPSRC funding from EP/P001645/1 Advanced Nuclear Materials. The authors acknowledge use of characterisation facilities within the David Cockayne Centre for Electron Microscopy, Department of Materials, University of Oxford, alongside financial support provided by the Henry Royce Institute (Grant ref EP/R010145/1) and the LEAP 5000 XR (EP/M022803/1). We also acknowledge funding by the UKRI Energy Programme (Grant No. EP/T012250/1).

Data Statement

~~A full list of the experimental data used in this work can be found in the supplementary information. Some of the data used in this study cannot be made available due to proprietary reasons. The rest of the data and scripts can be found here https://ora.ox.ac.uk/objects/uuid:94ff8767-a5e1-4c68-bae7-bb2016b97733 .~~

To aid the reproducibility of our work, wherever possible, datasets are provided in full within the Oxford Research Archive at the following URL https://ora.ox.ac.uk/objects/uuid:94ff8767-a5e1-4c68-bae7-bb2016b97733 . However, some of the data used in this study cannot be made available due to proprietary reasons. We have included a full list of the experimental datasets in the supplementary information and shown their availability.

References

BANERJEE, S. (2001). Nuclear Applications: Zirconium Alloys. *Encyclopedia of Materials: Science and Technology (Second Edition)* 6287–6299. http://www.sciencedirect.com/science/article/pii/B0080431526011177%5Cnhttp://ac.els-cdn.

BREEN, A. J., MOUTON, I., LU, W., WANG, S., SZCZEPANIAK, A., KONTIS, P., STEPHENSON, L. T., CHANG, Y., DA SILVA, A. K., LIEBSCHER, C. H., RAABE, D., BRITTON, T. B., HERBIG, M. & GAULT, B. (2018). Atomic scale analysis of grain boundary deuteride growth front in Zircaloy-4. *Scripta Materialia* **156**, 42–46. https://www.sciencedirect.com/science/article/pii/S1359646218304123.

BREEN, A. J., STEPHENSON, L. T., SUN, B., LI, Y., KASIAN, O., RAABE, D., HERBIG, M. & GAULT, B. (2020). Solute hydrogen and deuterium observed at the near atomic scale in high-strength steel. *Acta Materialia* **188**, 108–120.

CHEN, Y.-S., HALEY, D., GERSTL, S. S. A., LONDON, A. J., SWEENEY, F., WEPF, R. A., RAINFORTH, W. M., BAGOT, P. A. J. & MOODY, M. P. (2017). Direct observation of individual hydrogen atoms at trapping sites in a ferritic steel. *Science* **355**, 1196–1199. http://www.sciencemag.org/lookup/doi/10.1126/science.aal2418.

COUET, A., MOTTA, A. T. & COMSTOCK, R. J. (2014). Hydrogen pickup measurements in zirconium alloys: Relation to oxidation kinetics. *Journal of Nuclear Materials* **451**, 1–13.

https://www.sciencedirect.com/science/article/pii/S0022311514001081.

ENSOR, B., LUCENTE, A. M., FREDERICK, M. J., SUTLIFF, J. & MOTTA, A. T. (2017). The role of hydrogen in zirconium alloy corrosion. *Journal of Nuclear Materials* **496**, 301–312. http://linkinghub.elsevier.com/retrieve/pii/S0022311517308693.

GEMMA, R., AL-KASSAB, T., KIRCHHEIM, R. & PUNDT, A. (2009). APT analyses of deuterium-loaded Fe/V multi-layered films. *Ultramicroscopy* **109**, 631–636. http://linkinghub.elsevier.com/retrieve/pii/S0304399108002970.

HUDSON, D. (2011). 'Zirconium Oxidation on the Atomic Scale'. University of Oxford.

JIANG, W., LUSCHER, W. G., WANG, T., ZHU, Z., SHAO, L. & SENOR, D. J. (2020). A quantitative study of retention and release of deuterium and tritium during irradiation of γ-LiAlO2 pellets. *Journal of Nuclear Materials* **542**, 152532.

JOHNSON, L. J. S., THUVANDER, M., STILLER, K., ODÉN, M. & HULTMAN, L. (2013). Blind deconvolution of time-of-flight mass spectra from atom probe tomography. *Ultramicroscopy* **132**, 60–64.

JONES, C., TULI, V., SHAH, Z., GASS, M., BURR, P. A., PREUSS, M. & MOORE, K. L. (2021). Evidence of hydrogen trapping at second phase particles in zirconium alloys. *Scientific Reports* **11**, 4370.

KAUTZ, E. J., DEVARAJ, A., SENOR, D. J. & HARILAL, S. S. (2021). Hydrogen isotopic analysis of nuclear reactor materials using ultrafast laser-induced breakdown spectroscopy. *Optics Express* **29**, 4936. https://doi.org/10.1364/OE.412351.

KINGHAM, D. R. (1982). The post-ionization of field evaporated ions: A theoretical explanation of multiple charge states. *Surface Science* **116**, 273–301.

KUNIMUNE, Y., SHIMADA, Y., SAKURAI, Y., INOUE, M., NISHIDA, A., HAN, B., TU, Y.,

TAKAMIZAWA, H., SHIMIZU, Y., INOUE, K., YANO, F., NAGAI, Y., KATAYAMA, T. & IDE, T. (2016). Quantitative analysis of hydrogen in SiO2/SiN/SiO2 stacks using atom probe tomography. *AIP Advances* **6**, 045121. http://aip.scitation.org/doi/10.1063/1.4948558 (Accessed April 26, 2021).

LI, K., LIU, J., GROVENOR, C. R. M. & MOORE, K. L. (2020). NanoSIMS Imaging and Analysis in Materials Science. *Annual Review of Analytical Chemistry* **13**, 273–292. https://www.annualreviews.org/doi/10.1146/annurev-anchem-092019-032524.

LONDON, A. J. (2019). Quantifying Uncertainty from Mass-Peak Overlaps in Atom Probe Microscopy. *Microscopy and Microanalysis* **25**, 378–388.

LONDON, A. J., HALEY, D. & MOODY, M. P. (2017). Single-Ion Deconvolution of Mass Peak Overlaps for Atom Probe Microscopy. In *Microscopy and Microanalysis*vol. 23, pp. 300–306. Cambridge University Press.

MAUS, M., COTLET, M., HOFKENS, J., GENSCH, T., DE SCHRYVER, F. C., SCHAFFER, J. & SEIDEL, C. A. M. (2001). An experimental comparison of the maximum likelihood estimation and nonlinear least-squares fluorescence lifetime analysis of single molecules. *Analytical Chemistry* **73**, 2078–2086. https://pubs.acs.org/sharingguidelines.

MEISENKOTHEN, F., SAMAROV, D. V., KALISH, I. & STEEL, E. B. (2020). Exploring the accuracy of isotopic analyses in atom probe mass spectrometry. *Ultramicroscopy* **216**, 113018.

MEYER, J. C., GIRIT, C. O., CROMMIE, M. F. & ZETTL, A. (2008). Imaging and dynamics of light atoms and molecules on graphene. *Nature* **454**, 319–322. http://www.nature.com/articles/nature07094.

MOTTA, A. T., CAPOLUNGO, L., CHEN, L. Q., CINBIZ, M. N., DAYMOND, M. R., KOSS, D. A., LACROIX, E., PASTORE, G., SIMON, P. C. A., TONKS, M. R., WIRTH, B. D. & ZIKRY, M. A. (2019). Hydrogen in zirconium alloys: A review. *Journal of Nuclear Materials* **518**, 440–460. https://www.sciencedirect.com/science/article/pii/S0022311518316763.

MOTTA, A. T., COUET, A. & COMSTOCK, R. J. (2015). Corrosion of Zirconium Alloys Used for Nuclear Fuel Cladding. *Annu. Rev. Mater. Res* **45**, 311–43. www.annualreviews.org.

MOUTON, I., BREEN, A. J., WANG, S., CHANG, Y., SZCZEPANIAK, A., KONTIS, P., STEPHENSON, L. T., RAABE, D., HERBIG, M., BRITTON, T. BEN & GAULT, B. (2019). Quantification Challenges for Atom Probe Tomography of Hydrogen and Deuterium in Zircaloy-4. *Microscopy and Microanalysis* **25**, 481–488.

MÜLLER, M., SAXEY, D. W., SMITH, G. D. W. & GAULT, B. (2011). Some aspects of the field evaporation behaviour of GaSb. *Ultramicroscopy* **111**, 487–492.

PARDEDE, M., LIE, T. J., IQBAL, J., BILAL, M., HEDWIG, R., RAMLI, M., KHUMAENI, A., BUDI, W. S., IDRIS, N., ABDULMADJID, S. N., MARPAUNG, A. M., KARNADI, I., TANRA, I., LIE, Z. S., SUYANTO, H., KURNIAWAN, D. P., KURNIAWAN, K. H., KAGAWA, K. & TJIA, M. O. (2019). H-D Analysis Employing Energy Transfer from Metastable Excited-State He in Double-Pulse LIBS with Low-Pressure He Gas. *Analytical Chemistry* **91**, 1571–1577. https://pubs.acs.org/sharingguidelines.

SEPEHRI-AMIN, H., OHKUBO, T., NISHIUCHI, T., HIROSAWA, S. & HONO, K. (2011). Quantitative laser atom probe analyses of hydrogenation-disproportionated Nd-Fe-B powders. *Ultramicroscopy* **111**, 615–618. http://linkinghub.elsevier.com/retrieve/pii/S0304399110003050.

SHARIQ, A., MUTAS, S., WEDDERHOFF, K., KLEIN, C., HORTENBACH, H., TEICHERT, S., KÜCHER, P. & GERSTL, S. S. A. (2009). Investigations of field-evaporated end forms in voltage- and laser-pulsed atom probe tomography. *Ultramicroscopy* **109**, 472–479.

SUNDELL, G., THUVANDER, M. & ANDRÉN, H. O. (2013). Hydrogen analysis in APT: Methods to control adsorption and dissociation of H2. *Ultramicroscopy* **132**, 285–289.

TAKAHASHI, J., KAWAKAMI, K., KOBAYASHI, Y. & TARUI, T. (2010). The first direct observation of hydrogen trapping sites in TiC precipitation-hardening steel through atom probe tomography. *Scripta Materialia* **63**, 261–264. https://www.sciencedirect.com/science/article/pii/S1359646210001508.

THOMPSON, K., LAWRENCE, D., LARSON, D. J., OLSON, J. D., KELLY, T. F. & GORMAN, B. (2007). In situ site-specific specimen preparation for atom probe tomography. *Ultramicroscopy* **107**, 131–139.

TSONG, T. T., KINKUS, T. J. & AI, C. F. (1983). Field induced and surface catalyzed formation of novel ions: A pulsed-laser time-of-flight atom-probe study. *The Journal of Chemical Physics* **78**, 4763–4775. http://aip.scitation.org/doi/10.1063/1.445276.

WADMAN, B., ANDRÉN, H.-O. & ROLANDER, U. (1988). Preferential Field Evaporation During Atom Probe Analysis of Zircaloy-4. *Journal de Physique* **C6**, 323–327. https://hal.archives-ouvertes.fr/jpa-00228153.

Tables

Table 1: Composition of ZIRLO dataset of the whole mass spectrum. This data is modelled on the 0.6 nJ section from the laser energy optimisation experiment.

Element	Zr	H	Nb	Sn	Al	Fe
Composition (at.%)	82.53	16.34	0.34	0.77	0.01	<0.01

Table 2: Composition of ZIRLO data for the Zr 2+ peaks only. This data is modelled on the 0.6 nJ section from the laser energy optimisation experiment

Element	Zr	H	Nb
Composition (at.%)	85.5	14.26	0.24

Table 3: Compositions calculated by each software package for real and Gaussian peak shapes

Element	Composition (at.%)								
	Simulated (True)	Real Peak Shape				Gaussian Peak Shape			
		AtomProbeLab	Deviation from simulated	IVAS	Deviation from simulated	AtomProbeLab	Deviation from simulated	IVAS	Deviation from simulated
Zr	82.53	82.27	-0.26	82.54	+0.01	82.57	+0.04	82.56	+0.03
H	16.34	16.56	+0.22	16.28	-0.06	16.31	-0.03	16.31	-0.03
Nb	0.34	0.40	+0.06	0.39	+0.05	0.34	0.00	0.34	0.00
Fe	0.01	0.00	-0.01	0.02	+0.01	0.00	-0.01	0.00	-0.01
Al	0.01	0.01	0.00	0.01	0.00	0.01	0.00	0.01	0.00
Sn	0.77	0.77	0.00	0.76	-0.01	0.77	0.00	0.76	-0.01

Figure Legends

Figure 1: Variation in Nb concentration calculated using different methods. The error bars correspond to 90% confidence intervals for the maximum likelihood calculation.

Figure 2: Labelled sections of Zirlo mass spectrum with the species with ions in each peak marked. (a) Zr 2+ peaks from 45-50 Da. (b) Zr 1+ peaks. The height of the small vertical bars corresponds to the isotopic abundance of each ion.

Figure 3: Simulated mass spectra with Gaussian shaped peaks of different widths. The top row shows the mass spectra with Gaussian curves fitted. The bar charts give the fraction of counts in each peak as calculated using the fitted spectra, AtomProbeLab and IVAS.

Figure 4: Reconstruction showing location of metal and region over which the line profile was calculated. The arrow indicated the direction in which the line profile was taken.

Figure 5: Peak overlapped solved line profile across zirconium matrix- deuteride interface. The upper and lower bounds were calculated using the upper and lower limits of H_2:H ratio ($\mu \pm 2\sigma$) of 0.11 and 0.71. The error bars are the confidence intervals (90%) of the overlap solving calculation.

Figure 6: (a) and (b) 40 million atom sub-volume of representative H and D charged Zircalloy-4 datasets respectively showing relative density of ions originating from the peak at 1 Da, 2 Da and the relative electric field as measured from the charge state ratio between Zr^{3+} and Zr^{2+} peaks. The small red cube in the bottom left hand corner of the volumes represents the size of the voxels used in this calculation (3 nm x 3 nm x 3 nm). (c) The average measured 2 Da/1 Da vs. relative electric field measured for

each voxel – shaded error regions correspond to ± 2 standard deviations. The relative fields are an indication only.

Figures

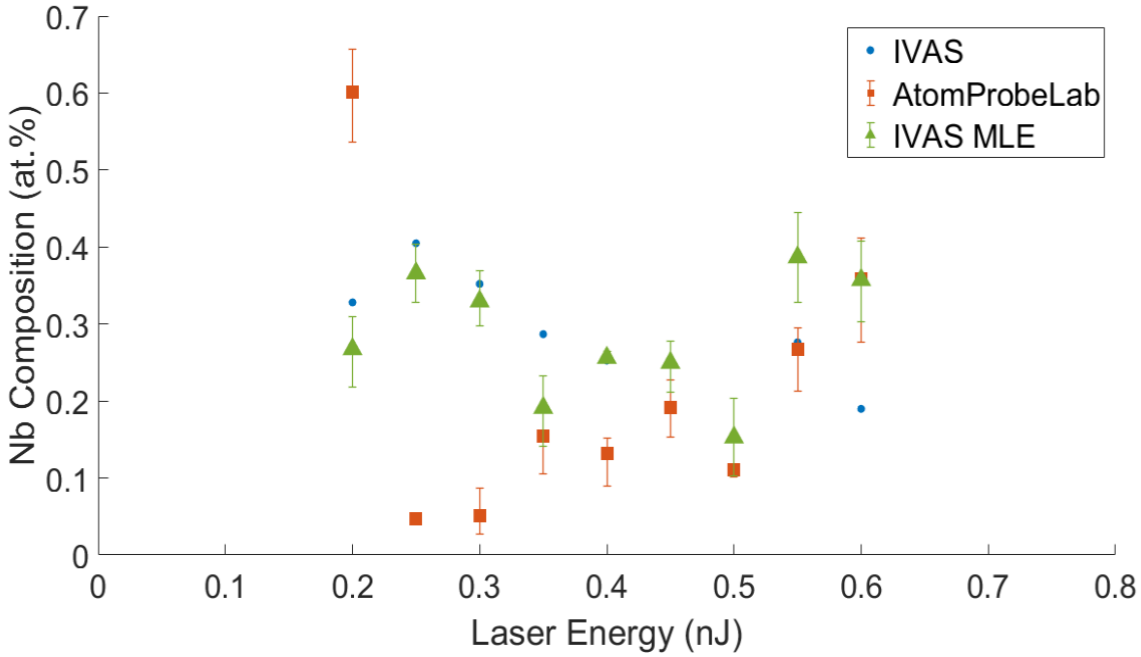

Figure 1

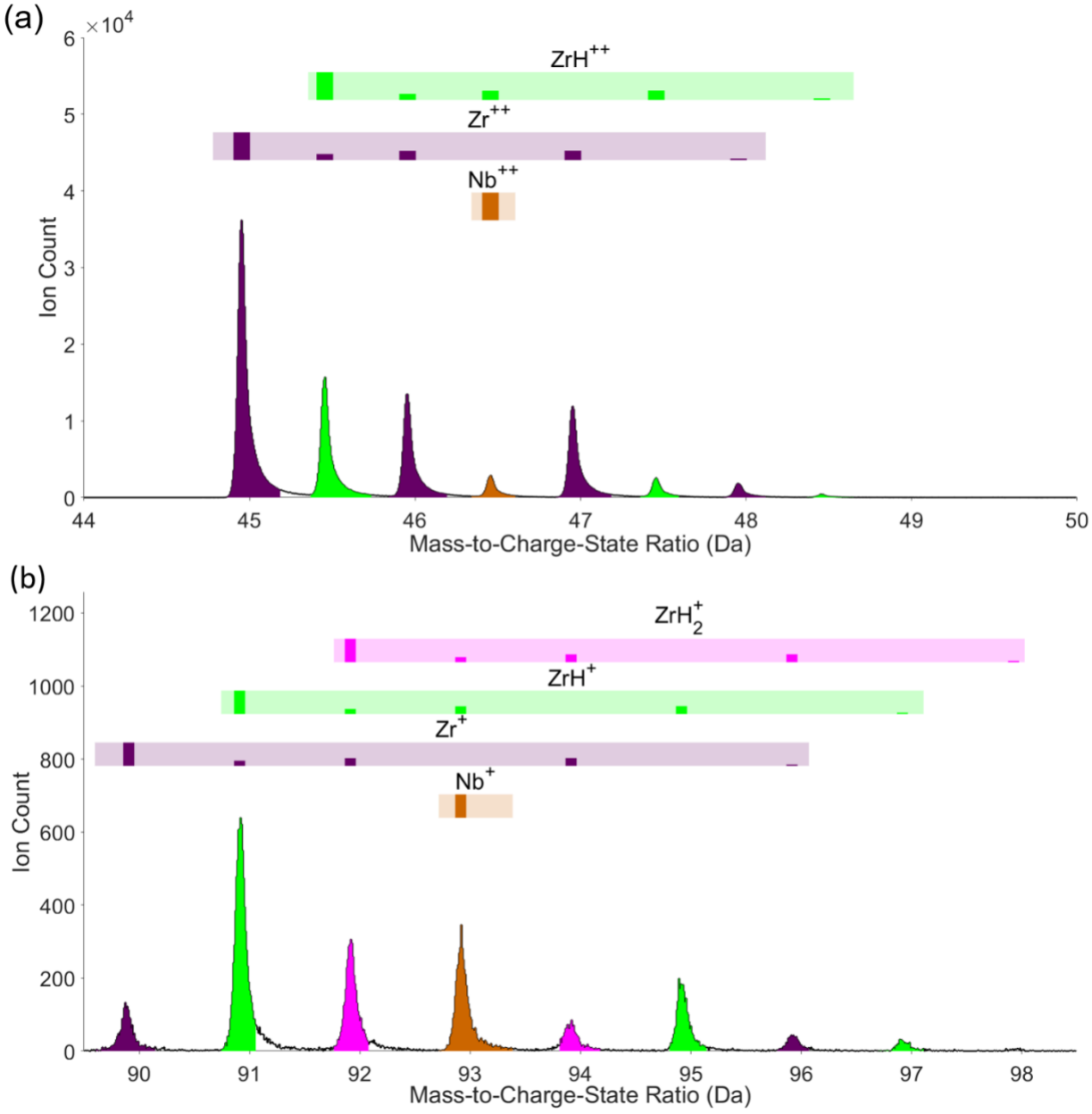
(a)
×10^4
6
5
4
3
2
1
0
ZrH++
Zr++
Nb++
Ion Count
44
45
46
47
48
49
50
Mass-to-Charge-State Ratio (Da)
(b)
1200
1000
800
600
400
200
0
ZrH2+
ZrH+
Zr+
Nb+
Ion Count
90
91
92
93
94
95
96
97
98
Mass-to-Charge-State Ratio (Da)

Figure 2

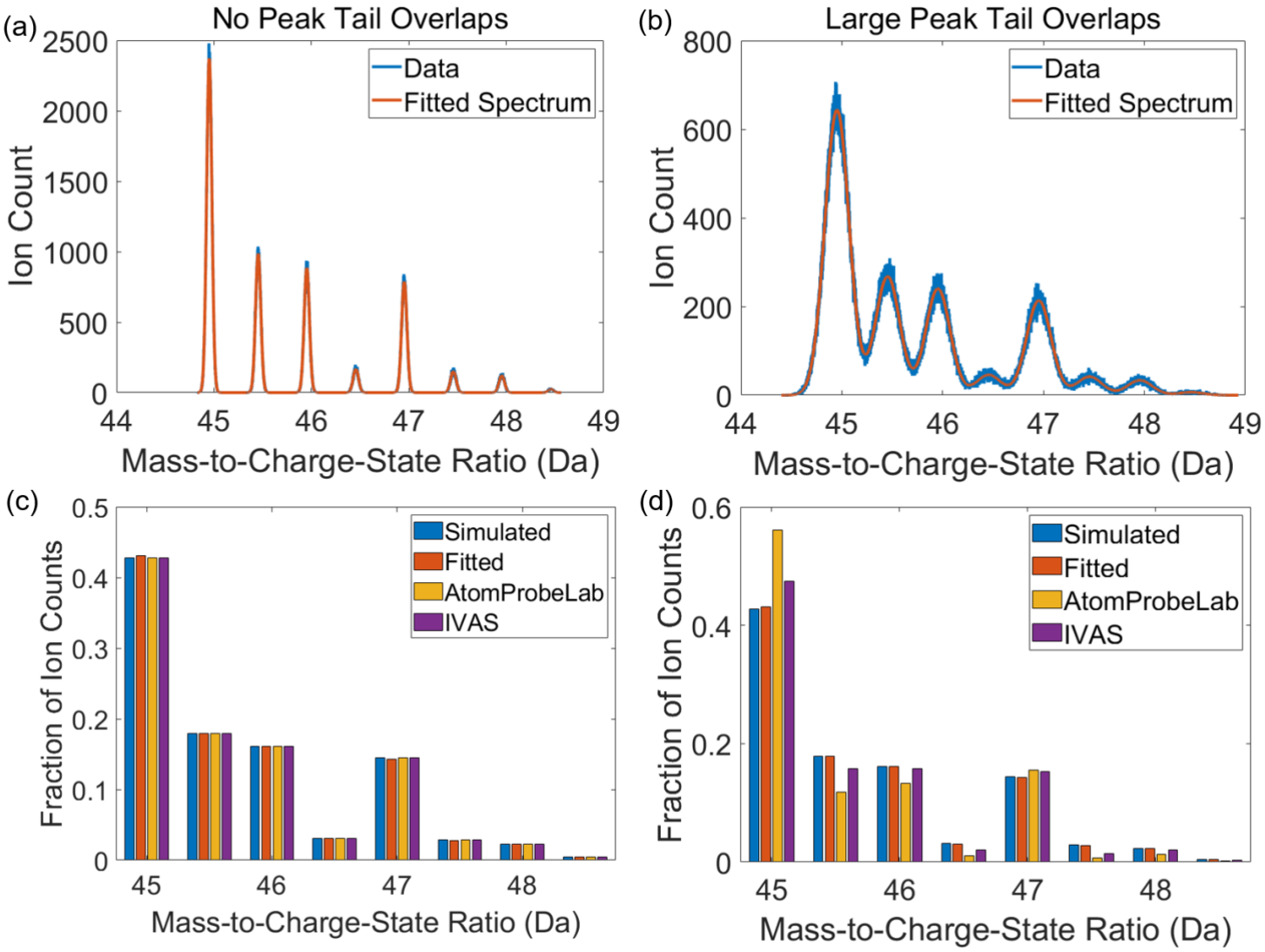
(a)
No Peak Tail Overlaps
Data
Fitted Spectrum
Ion Count
Mass-to-Charge-State Ratio (Da)
(b)
Large Peak Tail Overlaps
Data
Fitted Spectrum
Ion Count
Mass-to-Charge-State Ratio (Da)
(c)
Simulated
Fitted
AtomProbeLab
IVAS
Fraction of Ion Counts
Mass-to-Charge-State Ratio (Da)
(d)
Simulated
Fitted
AtomProbeLab
IVAS
Fraction of Ion Counts
Mass-to-Charge-State Ratio (Da)

Figure 3

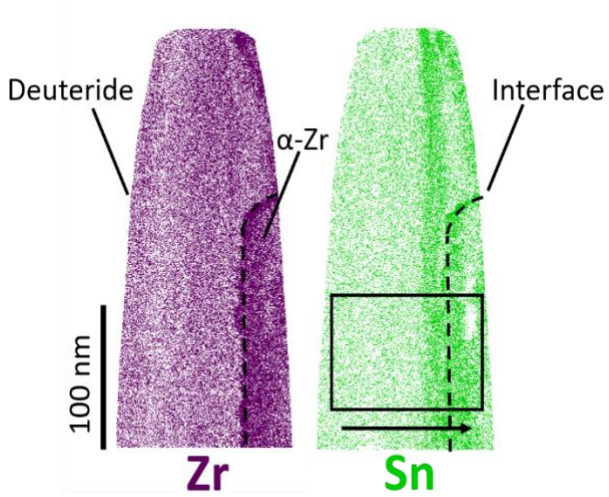

Figure 4

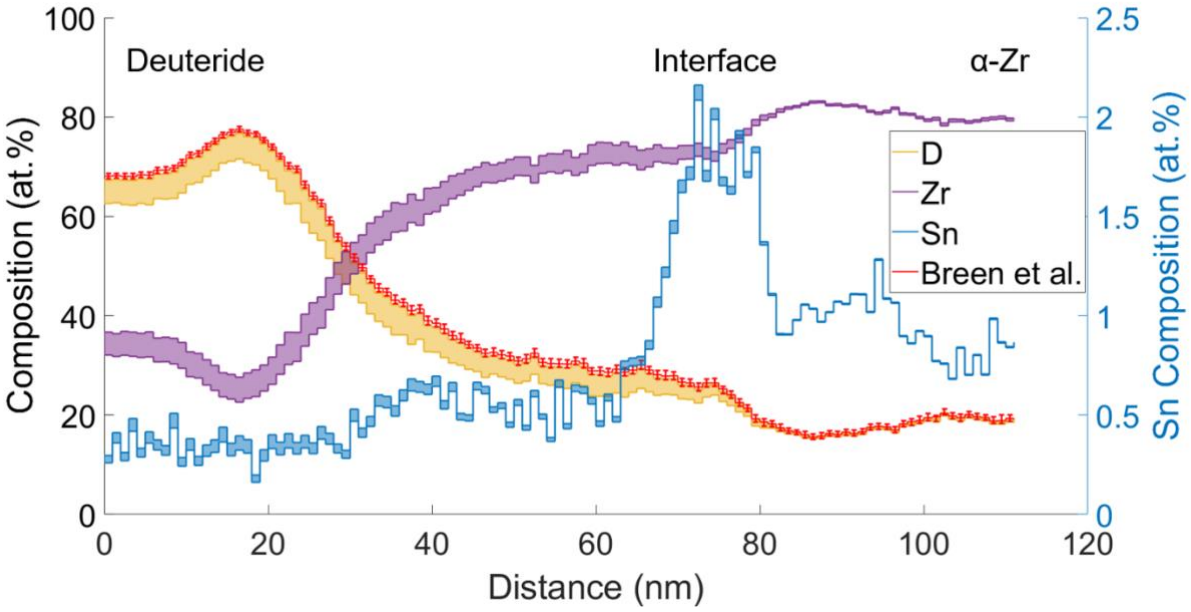
Deuteride
Interface
α-Zr
D
Zr
Sn
Breen et al.
Composition (at.%)
Sn Composition (at.%)
Distance (nm)
0
20
40
60
80
100
120
0
20
40
60
80
100
0
0.5
1
1.5
2
2.5

Figure 5

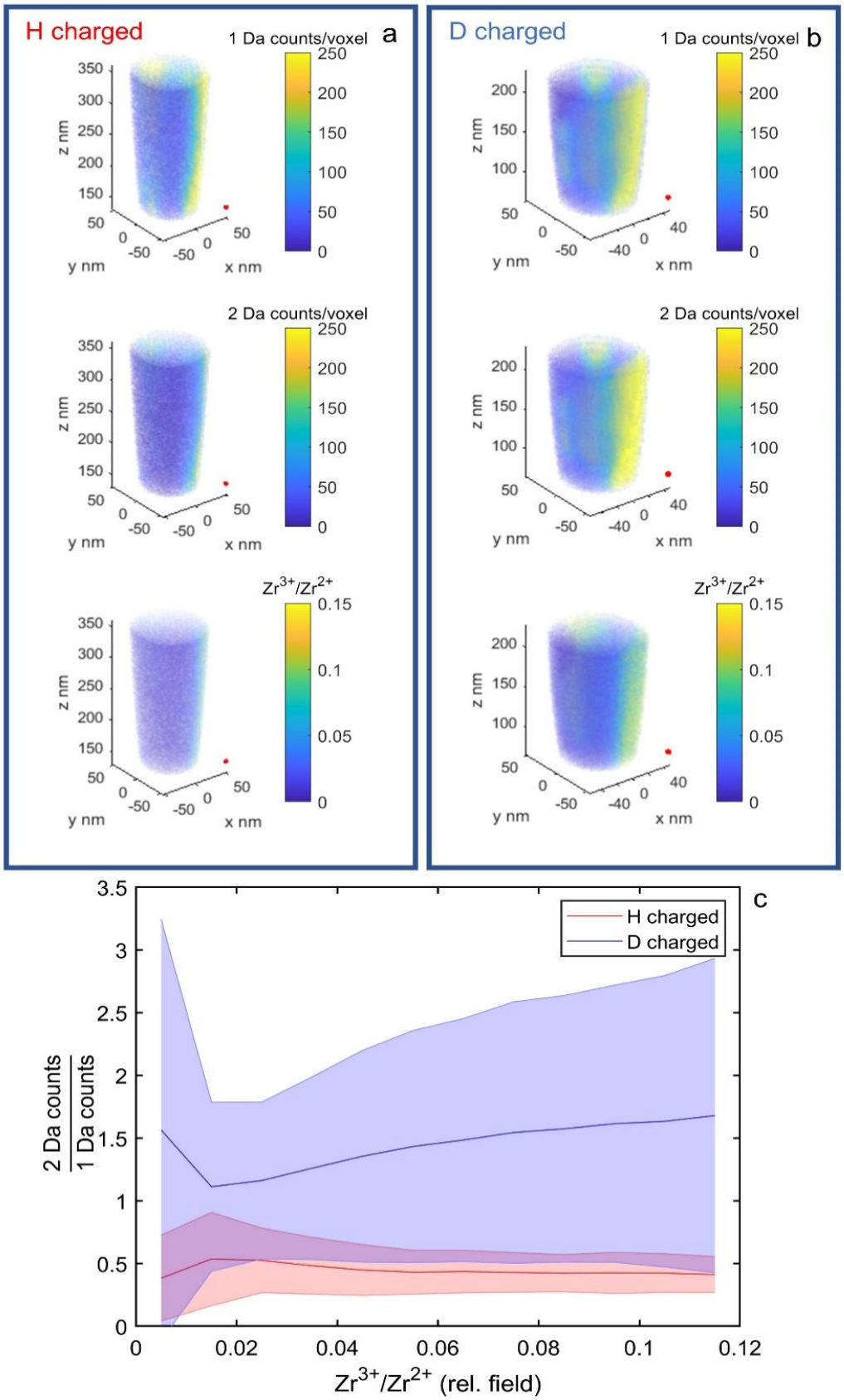
H charged
1 Da counts/voxel
a
2 Da counts/voxel
Zr3+/Zr2+
z nm
y nm
x nm
D charged
b
c
H charged
D charged
2 Da counts / 1 Da counts
Zr3+/Zr2+ (rel. field)

Figure 6